

## Optical characteristics of Al-doped ZnS thin film using pulsed laser deposition technique: the effect of aluminum concentration

A. A. Ahmed<sup>a,\*</sup>, O. Aldaghri<sup>b</sup>, E. Y. Salih<sup>c</sup>, A. Ramizy<sup>d</sup>, N Madkhali<sup>b</sup>,  
T. Alinad<sup>b</sup>, K. H. Ibnaouf<sup>b</sup>, M. H. Eisa<sup>a,b</sup>

<sup>a</sup>*Physics Department, College of Science, Sudan University of Science and Technology (SUST), Khartoum 11113, Sudan*

<sup>b</sup>*Department of Physics, College of Sciences, Imam Mohammad Ibn Saud Islamic University (IMSIU), Riyadh 13318, Saudi Arabia*

<sup>c</sup>*Department of medical Physics, College of Medical Sciences Technology, The University of Mashreq, 10021, Baghdad, Iraq*

<sup>d</sup>*Physics Department, College of Science, University of Anbar, Anbar, Iraq*

An efficient pulsed laser deposition (PLD) method was used to create un-doped and aluminum (Al) doped zinc sulfide (ZnS) nanomaterial. The effect of Al concentration on optical properties was investigated using two different techniques; namely, Ultra-violet visible light (UV-Vis) and Photoluminescence (PL) spectroscopies. Specifically, the optical analysis revealed a decrease in the optical bandgap values from 3.5 to 3.28 eV upon the addition of 8% of Al as dopant. While, the PL spectra of all samples showed a broad emission band in the 300-500 nm range. ZnS emission bands with Gaussian fitting are located at 396 and 459 nm. Despite from the pure ZnS peaks, three additional peaks at 345, 369, and 386 nm are observed for Al doped ZnS nanomaterial. Additionally, increasing the Al content up to 6% resulted in enhanced photoluminescence, but above this level, photoluminescence quenching was observed.

(Received March 11, 2022; Accepted June 1, 2022)

*Keywords:* ZnS: Al, PLD, UV-Vis, PL, Raman

### 1. Introduction

Nowadays, nanostructured inorganic structures and thin films are considered to be of great potential for general optoelectronic applications. Nanoparticles inorganic structures receives extensive attention in recent years because of their special properties [1-4]. To summarize the studies, zinc sulphide (ZnS) as nanoparticles materials was successfully used as important materials for the application in photovoltaic devices [5]. The ZnS is abundance, non-toxic, environmentally friendly and chemically stable natural material [6]. However, ZnS semiconductor material forms in two compound types of crystalline namely cubic zinc-blend (sphalerite) in a low temperature and Wurtzite in a high temperature [7, 8]. In addition, ZnS material exhibits a large bandgap in the proximity of (3.54-3.91 eV) for the zinc-blend and the wurtzite respectively [9, 10]. Moreover, ZnS material shows a large transmittance, high dielectric constant and high refractive index at the room temperature [10-12].

Additionally, based on demand, the physical properties of ZnS can be altered by dopant concentration [13-15]. ZnS doped with impurities are the most valuable process and thus exhibit different properties. Elements like, aluminum (Al), Indium (In), chromium (Cr), gallium (Ga), fluorine (F), copper (Cu), chlorine (Cl), boron (B) and manganese (Mn) with various doping levels can be applied to modified properties of ZnS [13-17]. Among these impurities, aluminum doped ZnS exhibits the excellent properties [18, 19]. As such, it is necessity to study the characteristics of ZnS nanomaterials under Al dopant concentration. Irrespective, the literature offers limited research focusing on the effects of under Al dopant concentration on the properties of ZnS nanomaterials deposited onto soda-lime glass substrate. Consequently, there is a need for

---

\* Corresponding author: [gostaaagogy@hotmail.com](mailto:gostaaagogy@hotmail.com)  
<https://doi.org/10.15251/CL.2022.196.381>

alternative materials that are cheaper with high performance like soda-lime glass. The multiple techniques used to prepare ZnS thin films, which give them a variety of interesting physical properties. These techniques include: electron beam deposition, thermal evaporation, sputtering, sol-gel, pulsed laser deposition and chemical bath deposition [18, 20-26]. In fact, the pulsed laser deposition (PLD) technique is an adaptable method which demonstrates a great capability to produce complex doped ZnS films. In this attempt, this study elucidates a thorough optical investigation of Al-doped ZnS using PLD approach.

## 2. Experimental work

### 2.1. Thin film deposition procedure

All reagents and chemicals utilized in this study were purchased from Sigma-Aldrich. In a typical procedure, ZnS was thoroughly mixed with different concentrations of  $Al_2O_3$  at room temperature with a formula of  $Zn_{1-x}Al_xS$  for ( $0 \leq x \leq 0.06$ ) where  $x$  is the aluminum doping ratio. Subsequently, a pallet of diameter and thickness of 12.0 and 2.0 mm, respectively, was attained using a hydraulic press of 5.0 ton. The acquired pallet was then annealed at 1200.0 °C and then rushed for numerous hours in the air to form the PLD target of ZnS and Al-doped ZnS. The soda-lime glass, as a substrate, was placed inside a container filled with acidic surfactant solution and subsequently was immersed in an ultrasound bath for 10.0 minutes to remove any undesired contaminations. Hereinafter, the utilized substrate was risen in a beaker of de-ionized water (DI). Herein,  $Zn_{1-x}Al_xS$  films were deposited onto soda-lime glass substrate using PLD method under an oxygen gas partial pressure of  $10^{-3}$  torr. In particular, an Nd: YAG laser was utilized for this study with wavelength range of 255.0 nm to 1064.0 nm, laser energy of 100.0 mJ, pulse number of 500, pulse repetition rates of 10 ns, repetition frequency of 6 Hz, and laser fluence of 2.0 J/cm<sup>2</sup>. The laser was operated at pulse energy of 100.0 mJ, pulse number of 500.0. Additionally, the target-laser source distance was fixed at 12.0 cm with 45.0° angle, while the distance of the target to the substrate was fixed to 2.0 cm. Each deposited film was mounted on an x-y stage which in turn was controlled using a stepper motor.

### 2.2. Characterizations

The structural analysis of the deposited films was carried out using X-ray diffractometer (XRD, Bruker AXS D8) using Cu  $K\alpha$  radiation and acceleration voltage of 40 kV. Furthermore, the room temperature vibrational and structural investigation was recorded on WITec, Raman spectroscopy. While, the optical performance of the deposited films was studied using two different techniques; namely, ultraviolet visible light spectroscopy (Shimadzu, UV-Vis) and photoluminescence (model LS-50B, PL) spectrometers.

## 3. Results and discussion

Figure 1 (a) shows the XRD patterns of the deposited ZnS and ZnS:Al films with different dopant concentrations; the XRD spectra were recorded with scanning range of 5°-70°. It can be clearly noticed that the attained films exhibited amorphous phases nature. Additionally, a weak peak obtained at around  $2\theta = 28.4^\circ$  is mainly due to the occurrence of hexagonal structure (008) of ZnS; this in turn was found to be in a good accordance with the reported data (JCPDF card no: 39-1363) [27]. Moreover, the effect of Al dopant concentration can be investigated using the attained crystallite size using Debye Scherrer equation as well as FWHM (Figure 1, b). The latter can be considered as crystal quality indicator [28, 29]. As such, it can be clearly seen that higher dopant concentration resulted in higher crystallinity of the deposited films.

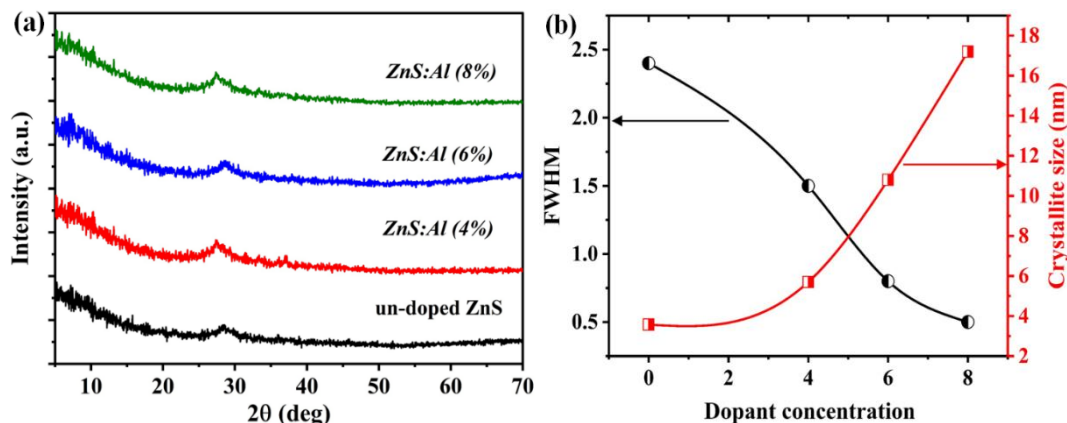


Fig. 1. Structural analysis of the deposited ZnS and ZnS:Al films; (a) XRD patterns and (b) crystal quality investigation.

Figure 2 illustrates the Raman spectra of the deposited films at different dopant concentrations. ZnS can be found in two polymorphs: cubic Zinc-blende and hexagonal wurtzite. The optical branches of cubic ZnS with two atoms per primitive unit cell are three-fold degenerate at  $K=0$ . However, due to the polarization field, the degeneracy collapses instantly away from the center of the Brillouin zone in ionic or partially ionic crystals. due to the obvious partial ionic nature of Zn-S bonding, both LO and TO modes are expected to be Raman active at  $k = 0$ .

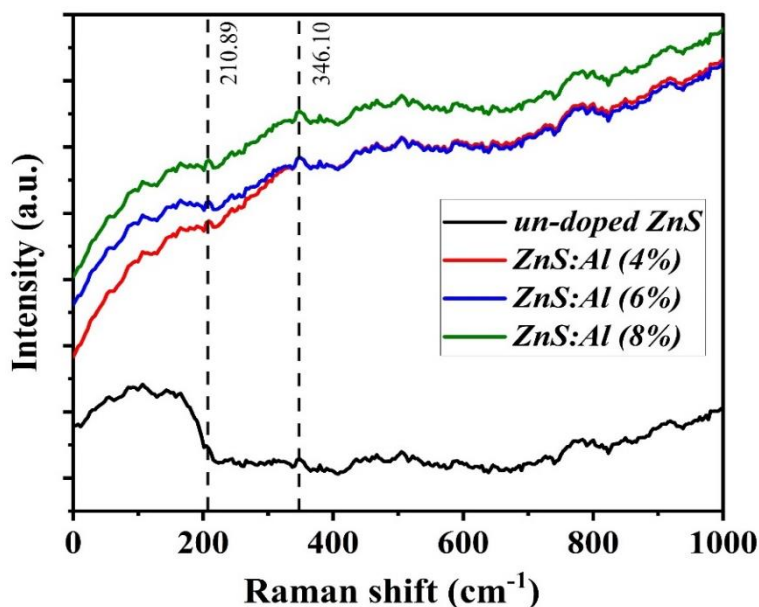


Fig. 2. Raman spectra of ZnS and ZnS:Al films.

As can be noticed in Figure 2, for each sample, the Raman spectrum displays the wave numbers of the associated phonon modes. The spectra of all ZnS:Al films show strong and broad peaks at  $210.86 \text{ cm}^{-1}$  and  $346.10 \text{ cm}^{-1}$ . A first-order TO mode of ZnS induces the peak at  $210.86 \text{ cm}^{-1}$ , and a cubic ZnS longitudinal optical (LO) phonon mode induces the peak near  $346.10 \text{ cm}^{-1}$  [30-32]. As a result, the Raman spectra showed the sample's structure as cubic ZnS. When compared to the Raman spectrum of pristine ZnS, the peaks of the first-order LO and TO phonon modes in the present samples shift towards lower energy (TO:  $271 \text{ cm}^{-1}$  and LO:  $352 \text{ cm}^{-1}$ ). The Raman peaks' softening and line broadening may be related to quantum confinement effects. The

nanoparticle size distribution and relaxation of the wave vector selection rule in these nanomaterials may result in a broadening and small shift of the TO and LO peaks. The intensity of the LO and TO modes increased slightly with increasing Al concentration in Al doped samples. This slight increase in intensity could be attributed to Al ions replacing Zn ions in the ZnS lattice. The ratio of the ionic radii of the host and dopant metals may be related to these changes. These could also be caused by new lattice defects or intrinsic host lattice defects created when Al ions enter Zn ion sites.

The optical analysis of the prepared samples, at different dopant concentration, is illustrated in Figure 3. Typically, all samples exhibited a cut-off absorption phenomenon at around 315 nm, with respect to the absorbance intensity (Figure 3, a). The aforementioned cut-off phenomenon could be due to the optical band gap of the deposited pristine ZnS film as well as the bathochromic shift (lower optical bandgap) of the attained ZnS: Al films, indicated using red arrows. This indicates the active role of Al as dopant in widening the absorption of the attained film. Additionally, the transmittance spectra of the deposited samples are depicted in Figure 3 (b). It can be clearly observed that the deposited films possess high intensity over the visible light region wherein lower transmission intensity was obtained at higher Al doping concentration. This in turn could be due to, to a certain extent, roughing surface at high dopant ratio [19]. It is also worth mentioning that higher intensity was noticed at higher wavelength region of the visible light.

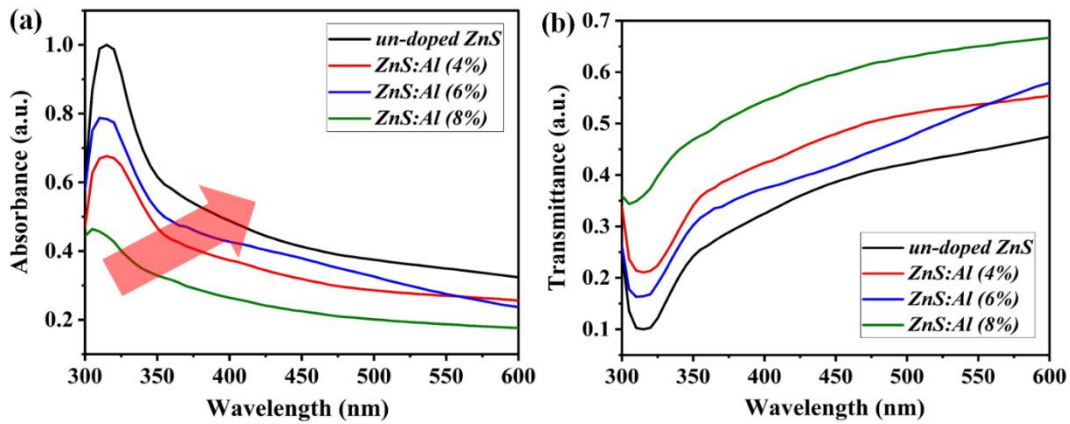


Fig. 3. (a) absorbance and (b) transmittance spectra of the deposited ZnS and ZnS: Al films.

Continuously, the optical bandgap of the fabricated films was calculated using Tuac relation [33]:

$$(\alpha h\nu) = A(h\nu - E_g)^{1/n} \quad (1)$$

The obtained results are demonstrated in Figure 4. Pristine ZnS exhibited an optical bandgap of 3.5 eV (Figure 4, a), which is mainly due to crystal structure of the prepared ZnS [19]. Continuously, a decrease in the estimated optical bandgap was noticed along with increasing the dopant concentration. This was found to be in an upright agreement with the XRD outcomes (Figure 1, b). In fact, such a phenomenon could be attributed to the electron transition from the valence band to the conduction band, as illustrated in the absorbance spectrum, as well as shrinking in the attained optical bandgap. Al doping resulted in decreasing the optical bandgap from 3.5 eV (Figure 4, a) to 3.28 eV (Figure 4, d).

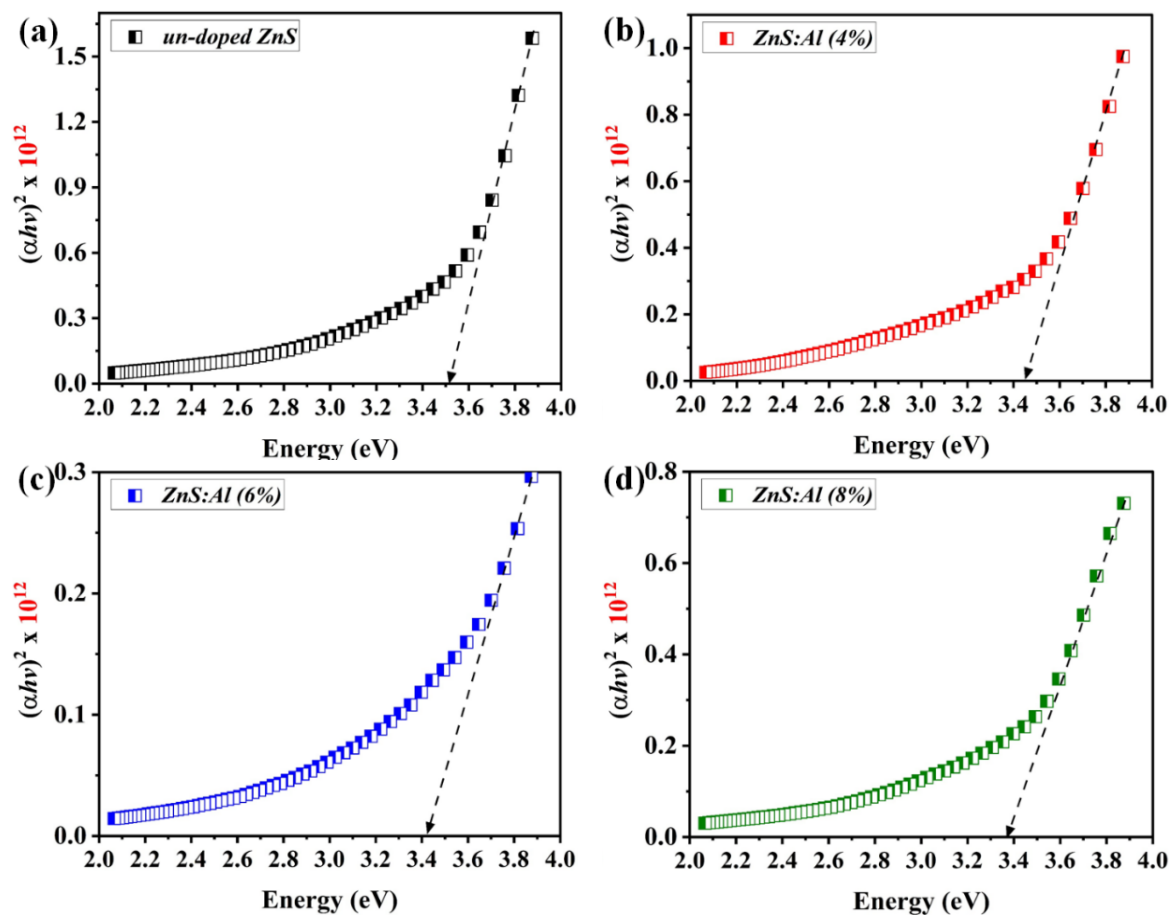


Fig. 4. optical bandgap of the deposited (a) pristine ZnS and (b-d) ZnS:Al at different dopant concentrations.

Spectra of Photoluminescence (PL) contain a broad UV emission band ranging 300-500 nm (Figure 4). Broad and asymmetric emission spectra indicate that several peaks may be superposition. These peaks were resolved using Gaussian fitting.

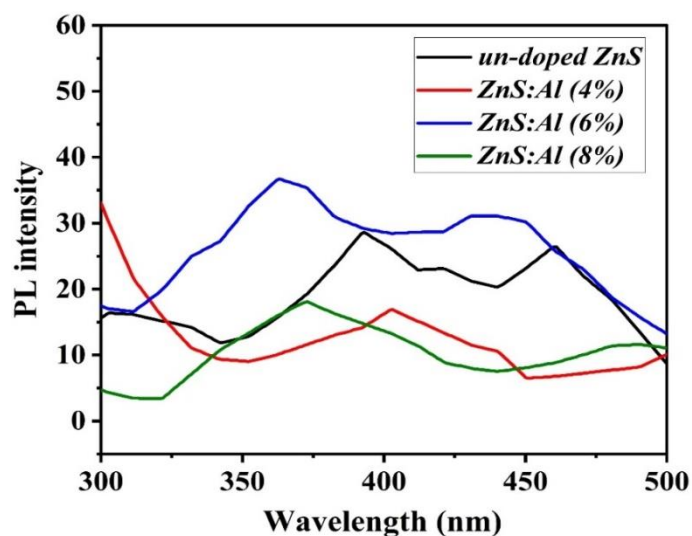


Fig. 4. PL spectra of pristine ZnS and ZnS: Al at different dopant concentration.

As shown in Figure 5 (a), the Gaussian fitting revealed emission bands at 396 and 459 nm. The luminescence peak at 396 nm can be attributed to zinc interstitials rather than sulfur interstitials. Because the sulfur ion has a larger ionic radius (1.7 Å) than the zinc ion (0.74 Å), it causes more strain in the ZnS lattice and the electron levels caused by the sulfur ion should have lower binding energies. Interstitial sulfur energy levels must therefore be closer to the conduction band than interstitial zinc energy levels [34]. Surface sulfur should have lower binding energies than internal sulfur vacancy states due to surface effects. As a result, the luminescence peak at 426 nm can be attributed to surface sulfur vacancies, i.e., electron recombination at the surface sulfur vacancy with holes in the valence band [35]. The emission band at 459 nm is attributed to the intrinsic emission of defects, vacancy, and the incorporation of trapped electrons by defects at the donor level under conduction range conditions [36].

The addition of dopant ions to the ZnS lattice changes the photoluminescence emission intensity and position of the PL peak. Figure 5 (b) illustrates a typical Gaussian fitting of the PL data of ZnS: Al (6%) film. The emission bands are located at 345, 369, and 386, as shown in the figure. In addition to the pure ZnS peaks, three additional peaks at 345, 369, and 386 nm are observed in Al doped samples. The PL positions at 369 and 386 nm could be attributed to self-activated luminescence caused by the incorporation of Al into the ZnS structure as a result of the donor-acceptor pair (DAP) transition [37].

This observation also provides evidence for the substitution of Al in the host lattice. Furthermore, a significant luminescence enhancement was observed in Al doped samples when compared to undoped ZnS samples. The increased emission caused by Al doping can be attributed to the following factors. **(i)** it is completely obvious that Al acts as a sensitizer, enhancing the radiative recombination processes. As a result, the photoluminescence efficiencies of ZnS: Al samples exceed those of ZnS samples. **(ii)** doping of donor impurities increases the electron population in the conduction band. **(iii)** increased donor-bound excitonic recombination and **(iv)** increased Sulphur vacancies caused by the addition of Al. All of these factors could have played a role in the increased luminescence. The intensity of the visible emission peaks for samples with  $x = 0.06$ , then decreases with increasing Al doping concentration. Most of the Al ions may have been incorporated into the ZnS lattice through substitution at  $x = 0.06$ ; however, at higher concentrations, the excess Al ions may have been incorporated into the nanomaterial's interstitially, resulting in more lattice defects. As a result, as the concentration of Al doping increases, the photoluminescence intensity decreases.

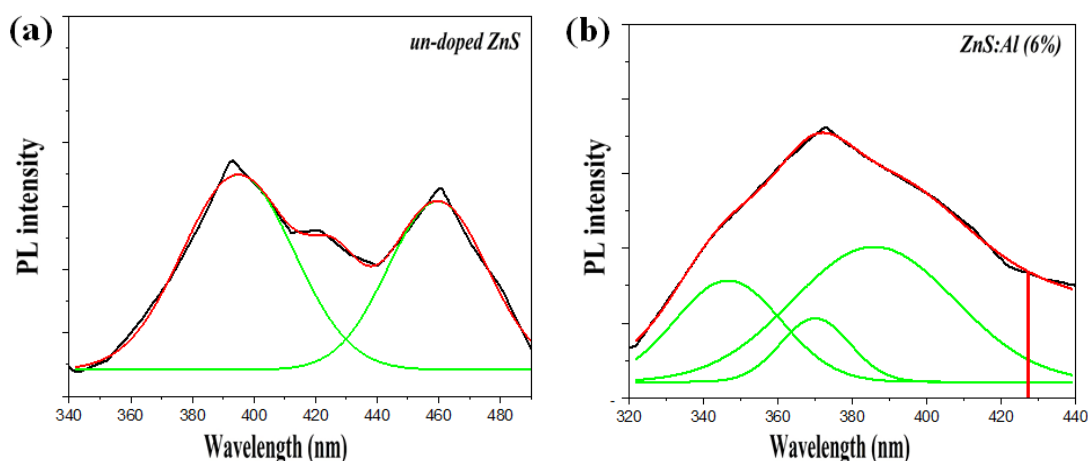


Fig. 5. Gaussian fit (red) of experimental PL (black) of (a) pristine ZnS and (b) ZnS:Al (6%); the green curves represent the deconvoluted peaks.

#### 4. Conclusion

Un-doped and Al doped ZnS film, at different concentrations, were successfully fabricated using PLD approach. Subsequently, an in-depth investigation concerning the optical analysis of the addressed samples was attained. In particular, the UV-Vis analysis the active role of Al as a dopant in decreasing the optical bandgap from 3.5 to 3.28 eV. The Photoluminescence for all of the samples showed a wide emission band in the 300-500 nm range. ZnS emission bands with Gaussian fitting are located at 396 and 459 nm. In addition to the pure ZnS peaks, several more peaks at 345, 369, and 386 nm are observed for Al doped ZnS nanoparticles. The pulsed laser deposition method was used to synthesize AZS. Enhanced photoluminescence, as the concentration of Al doping increases, the PL intensity decreases.

#### Acknowledgements

The authors express their gratitude to the Deanship of Scientific Research at Imam Mohammad Ibn Saud Islamic University which funded their work via Research Group no. RG-21-09-44.

#### References

- [1] E.Y. Salih, M.B.A. Bashir, A.H. Rajpar, I.A. Badruddin, *Ceramics International*, (2021); <https://doi.org/10.1016/j.ceramint.2021.12.203>
- [2] E.Y. Salih, M.F.M. Sabri, M.H. Eisa, K. Sulaiman, A. Ramizy, M.Z. Hussein, S.M. Said, *Materials Science in Semiconductor Processing*, 121 (2021) 105370; <https://doi.org/10.1016/j.mssp.2020.105370>
- [3] J. Jeevanandam, A. Barhoun, Y.S. Chan, A. Dufresne, M.K. Danquah, *Beilstein journal of nanotechnology*, 9 (2018) 1050-1074; <https://doi.org/10.3762/bjnano.9.98>
- [4] A.S. Mohammed, O.A. Fahad, A. Ramizy, E.Y. Salih, *Ceramics International*, 47 (2021) 17907-17914; <https://doi.org/10.1016/j.ceramint.2021.03.103>
- [5] Y. Bouznit, Y. Beggah, A. Boukerika, A. Lahreche, F. Ynineb, *Applied surface science*, 284 (2013) 936-941; <https://doi.org/10.1016/j.apsusc.2013.03.155>
- [6] D.H. Hwang, J.H. Ahn, K.N. Hui, K. San Hui, Y.G. Son, *Nanoscale research letters*, 7 (2012) 1-7; <https://doi.org/10.1186/1556-276X-7-26>
- [7] S. Ummartyotin, Y. Infahsaeng, *Renewable and Sustainable Energy Reviews*, 55 (2016) 17-24; <https://doi.org/10.1016/j.rser.2015.10.120>
- [8] J. Kennedy, P. Murmu, P. Gupta, D. Carder, S. Chong, J. Leveneur, S. Rubanov, *Materials science in semiconductor processing*, 26 (2014) 561-566; <https://doi.org/10.1016/j.mssp.2014.05.055>
- [9] J. Cheng, D. Fan, H. Wang, B. Liu, Y. Zhang, H. Yan, *Semiconductor science and technology*, 18 (2003) 676; <https://doi.org/10.1088/0268-1242/18/7/313>
- [10] N. Kaur, S. Kaur, J. Singh, M. Rawat, *J Bioelectron Nanotechnol*, 1 (2016) 1-5; <https://doi.org/10.13188/2475-224X.1000006>
- [11] X. Fang, T. Zhai, U.K. Gautam, L. Li, L. Wu, Y. Bando, D. Golberg, *Progress in Materials Science*, 56 (2011) 175-287; <https://doi.org/10.1016/j.pmatsci.2010.10.001>
- [12] M.E. Pacheco, C.B. Castells, L. Bruzzone, *Sensors and Actuators B: Chemical*, 238 (2017) 660-666; <https://doi.org/10.1016/j.snb.2016.07.125>
- [13] A. Attaf, A. Derbali, H. Saidi, H. Benamra, M. Aida, N. Attaf, H. Ezzaouia, L. Derbali, *Physics Letters A*, 384 (2020) 126199; <https://doi.org/10.1016/j.physleta.2019.126199>
- [14] X. Zhang, D. Wu, X. Zhou, Y. Yu, J. Liu, N. Hu, H. Wang, G. Li, Y. Wu, *TrAC Trends in Analytical Chemistry*, 121 (2019) 115668; <https://doi.org/10.1016/j.trac.2019.115668>

- [15] A. Jrad, T.B. Nasr, N. Turki-Kamoun, *Journal of Materials Science: Materials in Electronics*, 26 (2015) 8854-8862; <https://doi.org/10.1007/s10854-015-3566-2>
- [16] T. Hurma, *Materials Science Poland*, 37 (2019) 599-606; <https://doi.org/10.2478/msp-2019-0072>
- [17] M.B.A. Bashir, M.F.M. Sabri, S.M. Said, Y. Miyazaki, I.A. Badruddin, D.A.A. Shnawah, E.Y. Salih, S. Abushousha, M.H. Elsheikh, *Journal of Solid State Chemistry*, (2020) 121205; <https://doi.org/10.1016/j.jssc.2020.121205>
- [18] H. Benamra, H. Saidi, A. Attaf, M. Aida, A. Derbali, N. Attaf, *Surfaces and Interfaces*, 21 (2020) 100645; <https://doi.org/10.1016/j.surfin.2020.100645>
- [19] A. Azmand, H. Kafashan, *Journal of Alloys and Compounds*, 779 (2019) 301-313; <https://doi.org/10.1016/j.jallcom.2018.11.268>
- [20] C. Bishop, *Vacuum deposition onto webs, films and foils*, William Andrew, 2011.
- [21] H. Fujioka, Pulsed laser deposition (PLD). *Handbook of crystal growth*, in, Elsevier, 2015; <https://doi.org/10.1016/B978-0-444-63304-0.00008-1>
- [22] D. Depla, S. Mahieu, J. Greene, Sputter deposition processes, in: *Handbook of deposition technologies for films and coatings*, Elsevier, 2010, pp. 253-296; <https://doi.org/10.1016/B978-0-8155-2031-3.00005-3>
- [23] K. Koparkar, *Plasma polymerized thin film sensor: Synthesis and application*, *Sensors & Transducers*, 143 (2012) 10.
- [24] D. Levy, M. Zayat, *The Sol-Gel Handbook*, 3 Volume Set: Synthesis, Characterization, and Applications, John Wiley & Sons, 2015; <https://doi.org/10.1002/9783527670819>
- [25] V. Kumar, M. Saroja, M. Venkatachalam, S. Shankar, Synthesis and characterization of ZnS thin films by solgel dip and spin coating methods, *Int.. J. Rec. Sci. Res*, 6 (2015) 7377-7379.
- [26] T. Schneller, R. Waser, M. Kosec, D. Payne, *Chemical solution deposition of functional oxide thin films*, Springer, 2013; <https://doi.org/10.1007/978-3-211-99311-8>
- [27] K.H. Maria, P. Sultana, M. Asfia, *AIP Advances*, 10 (2020) 065315; <https://doi.org/10.1063/5.0011191>
- [28] F. Salleh, R. Usop, N.S. Saugi, E.Y. Salih, M. Mohamad, H. Ikeda, M.F.M. Sabri, M.K. Ahmad, S.M. Said, *Applied Surface Science*, 497 (2019) 143736; <https://doi.org/10.1016/j.apsusc.2019.143736>
- [29] M.B.A. Bashir, E.Y. Salih, M.F.M. Sabri, A.H. Rajpar, I.A. Badruddin, M.Z. Hussein, B.E. Al-Jumaili, In-Depth Thermal, *ECS Journal of Solid State Science and Technology*, 10 (2021) 106006; <https://doi.org/10.1149/2162-8777/ac2b3b>
- [30] K. Nagamani, N. Revathi, P. Prathap, Y. Lingappa, K.R. Reddy, *Current Applied Physics*, 12 (2012) 380-384; <https://doi.org/10.1016/j.cap.2011.07.031>
- [31] S. Acharya, N. Maheshwari, L. Tatikondewar, A. Kshirsagar, S. Kulkarni, *Crystal growth & design*, 13 (2013) 1369-1376; <https://doi.org/10.1021/cg301173k>
- [32] G. Rani, P. Sahare, *Spectroscopy Letters*, 46 (2013) 391-396; <https://doi.org/10.1080/00387010.2012.744318>
- [33] E.Y. Salih, A. Ramizy, O. Aldaghri, M.F. Mohd Sabri, N. Madkhali, T. Alinad, K.H. Ibnaouf, M.H. Eisa, *Crystals*, 12 (2022) 79; <https://doi.org/10.3390/cryst12010079>
- [34] C. Lan, K. Hong, W. Wang, G. Wang, *Solid state communications*, 125 (2003) 455-458; [https://doi.org/10.1016/S0038-1098\(02\)00914-6](https://doi.org/10.1016/S0038-1098(02)00914-6)
- [35] S. Wageh, Z.S. Ling, X. Xu-Rong, *Journal of Crystal Growth*, 255 (2003) 332-337; [https://doi.org/10.1016/S0022-0248\(03\)01258-2](https://doi.org/10.1016/S0022-0248(03)01258-2)
- [36] S.S. Kumar, M.A. Khadar, K. Nair, *Journal of luminescence*, 131 (2011) 786-789; <https://doi.org/10.1016/j.jlumin.2010.12.004>
- [37] D.A. Reddy, C. Liu, R. Vijayalakshmi, B. Reddy, *Journal of alloys and compounds*, 582 (2014) 257-264; <https://doi.org/10.1016/j.jallcom.2013.08.051>